PROGRESS OF MESH REDUCTION METHODS

XIAO-WEI GAO, HUA-YU LIU & WEI-LONG FAN
State Key Laboratory of Structural Analysis for Industrial Equipment, Dalian University of Technology, China

ABSTRACT
According to the discretization manner and manipulation dimensionality, numerical methods can be classified into two big groups, the full dimensionality method and mesh reduction methods. The former includes the finite element method, finite block method, element differential method and so on, and the latter can be further divided into three types: surface-based, line-based and point-based methods. The surface-based method consists of the boundary element method, finite volume method, boundary face method and so on; the line-based method includes the finite difference method, finite element line method, finite line method and so on; and the point-based method mainly consists of the mesh free method, fundamental solution method, free element method and so on. The paper gives a detailed description on the progress achieved in recent years in the mesh reduction methods, among which a brief introduction will go into the surface- and point-based methods and a detailed one will be given to the line-based methods, especially the finite line method (FLM). FLM is a new type collocation method, which has a distinct feature that the solution scheme to solve a partial differential equation is established by using two or three lines crossing a collocation point for 2D or 3D problems. The Lagrange polynomial formulation is used to approximate the variation of the coordinates and physical variables over each line. And the directional derivative technique is used to derive various orders spatial partial derivatives of any physical variables. The derived partial derivatives can be directly substituted into the governing partial differential equations and related boundary conditions to set up the discretized system of equations. An example will be given for the mechanical problem to demonstrate the accuracy and efficiency of the descripted mesh reduction methods.
Keywords: mesh reduction method, finite line method, collocation method, finite difference method, mesh free method.

1 INTRODUCTION

Most engineering problems can be represented by a set of second-order partial differential equations (PDEs) with proper boundary conditions (BC), which are constituted of the so called boundary value problems (BVP) of PDEs [1]. For example, the solid mechanics problem has the following BVP [2]:

$$\text{PDE:} \qquad \frac{\partial}{\partial x_l}\left(D_{ijkl}(\boldsymbol{x})\frac{\partial u_k(\boldsymbol{x})}{\partial x_j}\right)+b_i(\boldsymbol{x})=0, \quad \boldsymbol{x}\in\Omega, \tag{1}$$

$$\text{BC:} \qquad \begin{cases} u_i(\boldsymbol{x})=\overline{u}_i, & \boldsymbol{x}\in\Gamma_u \\ D_{ijkl}(\boldsymbol{x})n_j(\boldsymbol{x})\dfrac{\partial u_k(\boldsymbol{x})}{\partial x_l}=\overline{t}_i(\boldsymbol{x}), & \boldsymbol{x}\in\Gamma_t, \end{cases} \tag{2}$$

in which u_k is the displacement component, D_{ijkl} the stress–strain constitutive tensor, b_i the body force, and $\overline{t}_i$ the specified traction.

To solve the PDEs with a set of properly posed BC as listed above, a number of numerical methods are available, which can be globally divided into two big categories according to the geometry discretization and operation dimensions: the full dimensionality methods including the finite element method [3], finite block method [4], element differential method [2], and

WIT Transactions on Engineering Sciences, Vol 135, © 2023 WIT Press
www.witpress.com, ISSN 1743-3533 (on-line)
doi:10.2495/BE460091

so on, and mesh reduction methods including surface-based methods (i.e., the boundary element method [5], finite volume method [6], etc.), the line-based methods (i.e., the finite difference method [7], finite line method [8], etc.), and the point-based methods (i.e., the mesh free method [9], free element method [10], fundamental solution method [11], etc.). Most of these methods include two types of algorithms: weak-form and strong-form algorithms [9]. The weak-form algorithm needs integration over elements or divided sub-domains, and the strong-form algorithm usually is a type of collocation method without needing integration computation. In this paper, progresses in the mesh reduction methods are resumptively described.

A number of derivation techniques can be used to establish the solution schemes for above mentioned numerical methods. In view of the universal property, the weighted residual technique is used in the paper to establish the solution schemes for mesh reduction methods.

2 WEIGHTED RESIDUAL FORMULA FOR SOLVING PDES

Multiplying the PDE (1) on both sides with a weight function w and integrating it through the computational domain, it follows that:

$$\int_{\Omega} w(\boldsymbol{x}) \frac{\partial}{\partial x_l} \left(D_{ijkl}(\boldsymbol{x}) \frac{\partial u_k(\boldsymbol{x})}{\partial x_j} \right) d\Omega + \int_{\Omega} w(\boldsymbol{x}) b_i(\boldsymbol{x}) d\Omega = 0. \tag{3}$$

Taking integration by parts and applying the Gauss' divergence theorem to the first domain integral of eqn (3), the above equation becomes:

$$\int_{\Omega} \frac{\partial w(\boldsymbol{x})}{\partial x_l} D_{ijkl}(\boldsymbol{x}) \frac{\partial u_k(\boldsymbol{x})}{\partial x_j} d\Omega = \int_{\Gamma} w(\boldsymbol{x}) t_i(\boldsymbol{x}) d\Gamma + \int_{\Omega} w(\boldsymbol{x}) b_i(\boldsymbol{x}) d\Omega, \tag{4}$$

in which t_i is the traction component on the boundary Γ of the domain Ω, which has the relationship with the displacement gradient as shown in eqn (2).

In eqn (4), the basic physical variable u_k is mainly included in the volume integral of the left-hand side, so it is called the volume-based weighted residual formulation.

Taking integration by parts again to the first domain integral of eqn (4) and applying the Gauss' divergence theorem, the following equation can be resulted in:

$$\int_{\Gamma} \frac{\partial w}{\partial x_l} D_{ijkl} n_j u_k d\Gamma - \int_{\Omega} \frac{\partial}{\partial x_j} \left(D_{ijkl} \frac{\partial w}{\partial x_l} \right) u_k d\Omega = \int_{\Gamma} w t_i d\Gamma + \int_{\Omega} w b_i d\Omega. \tag{5}$$

In eqn (5), the basic physical variable u_k is included in both the surface and volume integrals of the left-hand side, so it is called the surface-volume-based weighted residual formulation.

From eqns (4) and (5), various weak-form solution algorithms can be generated by taking different kinds of the weight function *w*, such as the finite volume method and boundary element method.

3 SURFACE-BASED METHODS

The surface-based methods include the finite volume method (FVM) and boundary element method (BEM), which are operated mainly on the surfaces of a control volume or on the boundary of the considered problem.

3.1 Progress in FVM

The FVM seems to be a volume-based method. However, it is here classified into the category of the surface-based methods, because its main operation is over the surfaces rather than the volume. To see this, let us take the weight function w to be 1 in eqn (4) and thus it results in:

$$\int_{\Gamma} t_i \, d\Gamma + \int_{\Omega} b_i d\Omega = 0 . \tag{6}$$

In FVM, the computational domain is discretized into a serious of control volumes [12]. Applying eqn (6) to each control volume, say volume Ω_c, and dividing the boundary of Ω_c into two parts, the inner and out boundary parts, eqn (6) can be written as:

$$\int_{\Gamma_{Ic}} D_{ijkl} n_j \frac{\partial u_k}{\partial x_l} d\Gamma + \int_{\Gamma_{oc}} \overline{t}_i \, d\Gamma + \int_{\Omega_c} b_i d\Omega = 0, \tag{7}$$

where $\Gamma_{Ic} \cup \Gamma_{oc} = \partial\Omega_c$.

Eqn (7) is a typical formulation in FVM analysis, from which we can see that the main computation is over the control surfaces of a control volume. The key work in FVM is how to compute the physical variable gradient $\partial u_k / \partial x_l$ [13] included in the first control surface integral of eqn (7).

3.1.1 Conventional FVM

In the conventional FVM, the interface Γ_{Ic} is taken as the mid-surface connected by the collocation point c and around neighbour points, thus $\partial u_k / \partial x_l$ at the mid-surface can be easily computed by the values of u_k between c and the neighbour points [12], [13]. The point representing the physical variables may be the centre of a control volume (this being called the cell-centred FVM) or a vertex of an unstructured mesh (this being called the vertex-centred FVM) [14]. Figs 1 and 2 show two patterns of the vertex-centred FVM for a structured mesh and an unstructured mesh, respectively.

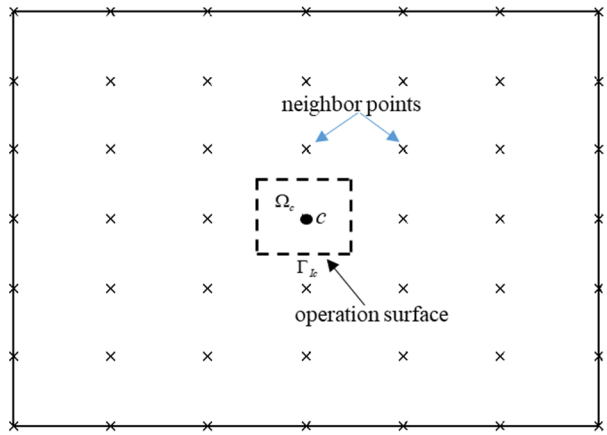

Figure 1: Operation surface formed by mid-points between collocation point c and neighbour points for a structural mesh.

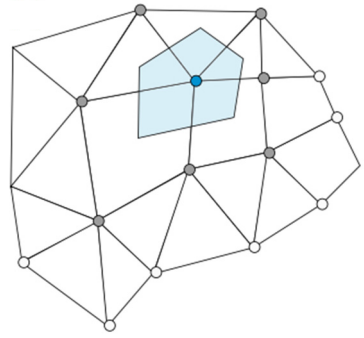

Figure 2: Control volume and its operation surface connected by mid-points between collocation point and neighbour vertices of an unstructured mesh [14].

Obviously, the linear variation of over the operation surface shown in Fig. 2 can be easily constructed, but it is difficult to construct a high-order scheme to compute the value of on the operation surface shown in Figs 1 and 2.

3.1.2 Free element based FVM (FEFVM)

In recent years, the authors proposed the free element method (FrEM) [10]. In the method, an isoparametric free element is defined at each collocation point as shown in Fig. 3. The weak-form formulation of FrEM has the form as shown in eqn (7), but a high-order control volume, the free element, can be easily formed as in FEM. The control surface in FEFVM is the boundary of the free element.

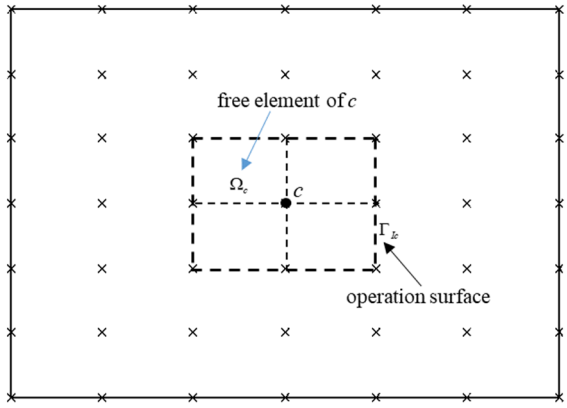

Figure 3: Operation surface formed by the boundary of the free element built for collocation point *c*.

Since high-order free elements can be easily formed in FrEM, the high accuracy of $\partial u_k / \partial x_l$ in FEFVM can also be easily achieved. A set of analytical expressions for computing $\partial u_k / \partial x_l$ over the formed free element was derived in Gao et al. [2]. Although it is easy to set up the solution scheme using the free element as shown in Fig. 3, the accuracy

of $\partial u_k / \partial x_l$ is not high. This is because its value is taken on the boundary of Ω_c, which is not as accurate as inside Ω_c. To improve the accuracy of $\partial u_k / \partial x_l$, the element-shell strengthened FVM is proposed in the following.

3.1.3 Element-shell strengthened FVM (ESFVM)

To improve the accuracy of $\partial u_k / \partial x_l$ included in the first boundary integral of eqn (7), additional free elements are formed for each side/surface of the collocation element Ω_c, which form an element ring/shell for a 2D/3D control sides/surfaces as shown in Fig. 4 for a 2D case.

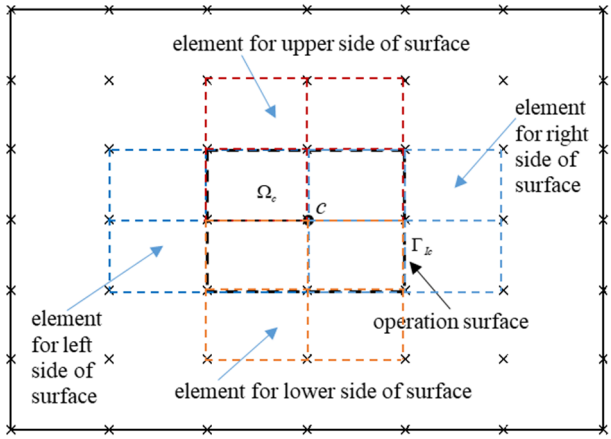

Figure 4: Additional elements around the operation surfaces.

In ESFVM, since the operation surfaces of Ω_c are included in the formed additional elements, the accuracy of $\partial u_k / \partial x_l$ is higher than using a same element as shown in Fig. (4).

3.2 Progress in BEM

In eqn (5), we take the weight function w as the displacement fundamental solution u^*_{mi} [5], that is $w = u^*_{mi}$, it follows that:

$$\int_\Gamma \frac{\partial u^*_{mi}}{\partial x_l} D_{ijkl} n_j u_k d\Gamma - \int_\Omega \frac{\partial}{\partial x_j}\left(D_{ijkl} \frac{\partial u^*_{mi}}{\partial x_l} \right) u_k d\Omega = \int_\Gamma u^*_{mi} t_i \, d\Gamma + \int_\Omega u^*_{mi} b_i d\Omega \,. \tag{8}$$

Because the fundamental solution u^*_{mi} satisfies the following equation:

$$\frac{\partial}{\partial x_j}\left(D_{ijkl} \frac{\partial u^*_{mi}}{\partial x_l} \right) + \delta_{mk}\delta(p,q) = 0 \,, \tag{9}$$

in which $\delta(p,q)$ is the Dirac function with p and q being the source and field points.

Substituting eqn (9) into eqn (8) yields the following integral equation:

$$u_m + \int_\Gamma t^*_{mk} u_k d\Gamma = \int_\Gamma u^*_{mi} t_i \, d\Gamma + \int_\Omega u^*_{mi} b_i d\Omega \,, \tag{10}$$

where:

$$t^*_{mk} = D_{ijkl} n_j \frac{\partial u^*_{mi}}{\partial x_l} \,. \tag{11}$$

For linear problems, the constitutive tensor D_{ijkl} is constant, therefore an analytical expression for the fundamental solution u^*_{mi} can be solved from eqn (9) [5]. However, for non-linear problems, D_{ijkl} is a function of unknown variables, the displacements or stresses. In this case, eqn (9) is unsolvable for u^*_{mi}. In order to solve such a problem, usually the fundamental solution for corresponding linear problems is employed and, as a result, the additional domain integrals may be generated in the integral eqn (10) [15] and in such cases the body force term b_i in eqn (10) should be understanded as a nominal body force.

To evaluate the domain integral involved in eqn (10), the conventional technique is to discretize the domain into internal cells [5], but this eliminates the advantage of BEM that only boundary of the problem needs to be discretized into elements. To overcome this drawback, people usually employ a transformation technique to transfer the domain integral into an equivalent one. The extensively used transformation technique is the dual reciprocity method (DRM) [16]. Another one is the radial integration method (RIM) [17] which can give more accurate results than DRM.

In RIM, the domain integral in eqn (10) can be expressed as:

$$\int_\Omega u^*_{mi} b_i d\Omega = \int_\Gamma \frac{F_{mi}}{r^n(p,q)} \frac{\partial r}{\partial n} d\Gamma(q), \tag{12}$$

in which the radial integral is:

$$F_{mi} = \int_0^{r(p,q)} u^*_{mi} b_i r^n dr, \tag{13}$$

where $n = 1$ for 2D and $n = 2$ for 3D problems, respectively. When b_i is a known function, eqns (12) and (13) can give an exact result. However, when b_i includes unknown quantities, such as the non-linear problems, b_i needs to be approximated first by a radial basis function [17] as in DRM, but this may reduce the computational accuracy.

4 LINE-BASED METHODS

The line-based methods include the conventional finite difference method (FDM) [7] and the recently proposed finite line method (FLM) [8]. In these methods, the computational domain is discretized into a series of points and lines to compute the spatial partial derivatives used in the PDEs are formed by around points. FDM constructs the first- and second-order partial derivatives by a line of points along the derivative direction. The main drawback in FDM is that if the lines of defining the derivative directions are not orthogonal each other in 2D or 3D problems, the accuracy of cross-partial derivatives of different directions usually is very poor. This is why FDM cannot well simulate the irregular geometry problems. In contrast, FLM has much better performance in overcoming this drawback.

FLM uses two or three lines (it is called as the line-set) at a collocation point to set up the solution scheme for 2D and 3D problems, as shown in Fig. 5 for a 2D case. Fig. 6 shows the high-order line-sets for an internal collocation point of 2D and 3D problems.

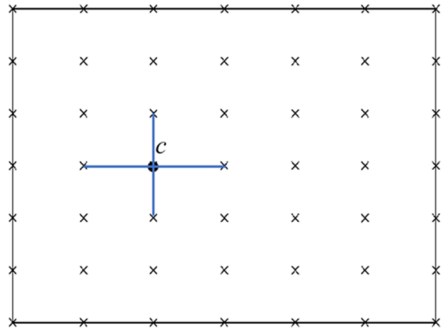

Figure 5: Line-set consisting of two crossed lines for a 2D problem.

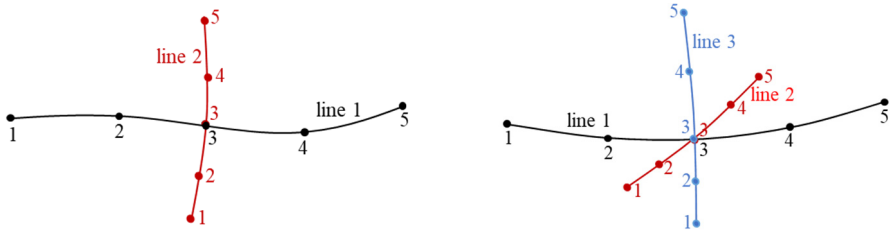

Figure 6: Node distribution over a line-set defined at a 2D and 3D internal point. (a) 2D problem; and (b) 3D problem.

Along a line of a line-set, the coordinates and physical variable can be expressed as:

$$x_i = \sum_{\alpha=1}^{m} L^{\alpha}(l) x_i^{\alpha} \equiv L^{\alpha}(l) x_i^{\alpha}, \tag{14}$$

$$u_k = \sum_{\alpha=1}^{m} L^{\alpha}(l) u_k^{\alpha} \equiv L^{\alpha}(l) u_k^{\alpha}, \tag{15}$$

in which m is the number of nodes defined along a line of the line-set, l is the arclength measured from node 1, and L^{α} is the Lagrange polynomial:

$$L^{\alpha}(l) = \prod_{\beta=1,\beta\neq\alpha}^{m} \frac{l - l^{\beta}}{l^{\alpha} - l^{\beta}}, \quad (\alpha = 1 \sim m). \tag{16}$$

By differentiating eqns (14) and (15) with respective to l, we can obtain the expressions of computing the first- and second-order partial derivatives at the collocation point $\boldsymbol{x}^c$ as follows [8]:

$$\frac{\partial u_k(\boldsymbol{x}^c)}{\partial x_i} = d_i^{c\alpha'} u_k^{\alpha'}, \tag{17}$$

$$\frac{\partial^2 u_k(\boldsymbol{x}^c)}{\partial x_i \partial x_j} = d_{ij}^{c\alpha''} u_k^{\alpha''}, \tag{18}$$

where:

$$d_i^{c\alpha'} = \sum_{I=1}^{d} [J]_{iI}^{-1} \left. \frac{\partial L_I^{\alpha'}(l)}{\partial l} \right|_{l=l(\boldsymbol{x}^c)}, \tag{19}$$

$$d_{ij}^{c\alpha''} = d_j^{c\beta'} d_i^{\beta'\alpha''}, \tag{20}$$

in which the repeated indexes represent summation, and $d = 2$ for 2D and $d = 3$ for 3D problems, I represents the line number.

Using eqns (17) and (18), we can easily discretize a PDE and related boundary conditions. For example, the PDE for the solid mechanics, shown in eqns (1) and (2) can be written as:

$$D_{ijkl}(\boldsymbol{x}^c) d_{lj}^{\alpha''} u_k^{\alpha''} + d_j^{\beta'} D_{ijkl}^{\beta'}(\boldsymbol{x}^c) d_l^{\alpha'} u_k^{\alpha'} + b_i(\boldsymbol{x}^c) = 0, \quad \boldsymbol{x}^c \in \Omega, \tag{21}$$

$$\begin{cases} u_k(\boldsymbol{x}^c) = \overline{u}_k(\boldsymbol{x}^c), & \boldsymbol{x}^c \in \Gamma_u \\ D_{ijkl}(\boldsymbol{x}^c) n_j(\boldsymbol{x}^c) d_l^{\alpha'} u_k^{\alpha'} = \overline{t}_i(\boldsymbol{x}^c), & \boldsymbol{x}^c \in \Gamma_t \end{cases}. \tag{22}$$

Using above discretized equations, a system of equations can be formed and solved for the displacement u_k at all collocation points.

5 POINT-BASED METHODS

The point-based methods cove a number of numerical methods, such as the mesh free method (MFM) [9], fundamental solution method (FSM) [18], radial basis function method [19] and the newly developed free element method (FrEM) [10]. In these methods, the computational domain is discretized into a series of points, and solution schemes are established by collocating the governing PDEs or its integral forms at each collocation point. In MFM, the partial derivatives at a collocation point c are derived based on a croup of points within a specified support region around c as shown in Fig. 7(a), while in FrEM, partial derivatives are derived based on an isometric free element formed for point c as shown in Fig. 7(b). In

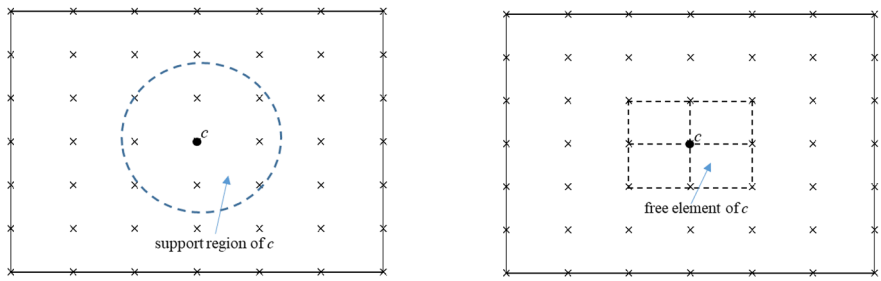

Figure 7: A 2D pattern for MFM (a); and FrEM (b) at a collocation point

MFM and FrEM, both strong-form and weak-form solution schemes are available. In the following, the two schemes of FrEM will be described in detail.

5.1 Strong-form free element method (SFrEM)

In FrEM, a free element as in FEM is independently formed for each collocation point. To easily facilitate forming high-order elements, the Lagrange polynomial element is usually adopted, and its shape functions for high-order dimensions can be straightforwardly formed by the 1D one, as follows [10]:

$$\begin{aligned} N_\alpha(\xi,\eta) &= L^I(\xi)L^J(\eta), && \text{for } 2D \\ N_\alpha(\xi,\eta,\zeta) &= L^I(\xi)L^J(\eta)L^K(\zeta), && \text{for } 3D, \end{aligned} \tag{23}$$

where the 1D shape functions L^I, L^J, and L^K are determined by eqn (16), and the superscript α is determined by the permutation of subscripts *I*, *J* and *K* sequentially.

The physical variable and its partial derivatives with respect to global coordinates can be derived as [2], [10]:

$$u_k = N_\alpha u_k^\alpha, \tag{24}$$

$$\frac{\partial u_k}{\partial x_i} = d_i^{c\alpha} u_k^\alpha, \quad \frac{\partial^2 u_k}{\partial x_i \partial x_j} = d_{ij}^{c\alpha} u_k^\alpha, \tag{25}$$

where:

$$\begin{aligned} d_i^{c\alpha} &= \frac{\partial N_\alpha}{\partial x_i} = [J]_{ik}^{-1} \frac{\partial N_\alpha}{\partial \xi_k}, \\ d_{ij}^{c\alpha} &= \frac{\partial^2 N_\alpha}{\partial x_i \partial x_j} = \left[[J]_{ik}^{-1} \frac{\partial^2 N_\alpha}{\partial \xi_k \partial \xi_l} + \frac{\partial [J]_{ik}^{-1}}{\partial \xi_l} \frac{\partial N_\alpha}{\partial \xi_k} \right] \frac{\partial \xi_l}{\partial x_j}, \end{aligned} \tag{26}$$

in which $[J]$ is the Jacobian matrix and its inverse and derivatives can be found in Gao et al. [2], [10] for details.

Similar to eqns (21) and (22), the discretized equations for setting up the system of equations can be directly obtained by substituting eqn (25) into eqns (1) and (2).

It is noted that the Lagrange elements shown in eqn (23) have the advantage of easily forming high-order elements. However, for problems with sharply changed geometries where the stress concentration may exist need finer points around these locations. For this type of problems, the weak-form FrEM can give more accurate results even if using coarse elements [20].

5.2 Weak-form free element method (WFrEM)

For a collocation point *c* with its free element being denoted as Ω_c, let us apply eqn (4) to Ω_c and the weight function is taken as the shape function of the collocation point *c* in eqn (24), that is $w = N_c$, from which the method is also called as the Galerkin FrEM [20], [21]. Thus, from eqn (4), it follows that:

$$\int_{\Omega_c} \frac{\partial N_c}{\partial x_l} D_{ijkl} \frac{\partial u_k}{\partial x_j} d\Omega = \int_{\partial\Omega_c} N_c t_i(\boldsymbol{x}) d\Gamma + \int_{\Omega_c} N_c b_i d\Omega, \tag{27}$$

in which the derivatives of the shape functions are computed using eqn (26).

Dividing the boundary $\partial\Omega_c$ of the free element Ω_c into two parts, the inner boundary Γ_{Ic} which is located within the problem and out boundary Γ_{oc} which is located on the out surface of the problem, and remembering that N_c is zero on the surfaces not including point *c* and this makes the integral over Γ_{Ic} zero, eqn (27) can be written as:

$$\int_{\Omega_c} \frac{\partial N_c}{\partial x_l} D_{ijkl} \frac{\partial N_\alpha}{\partial x_j} d\Omega\, u_k^\alpha = \int_{\Gamma_{oc}} N_c \overline{t_i}\, d\Gamma + \int_{\Omega_c} N_c b_i d\Omega, \tag{28}$$

where $\Gamma_{oc} = \partial\Omega_c \cap \partial\Omega$.

From eqn (28) it can be seen that the form of the basic equation in WFrEM is similar to that in the conventional FEM. However, there is an essential difference between them that the element in WFrEM is freely formed at each collocation point, and elements formed for different points are free each other without the restriction of nodal consistency between adjacent elements as in FEM. It is also noted that the elements formed for adjacent collocation points are overlapped in WFrEM, since they are formed locally and independently at each point.

6 NUMERICAL EXAMPLES

In this section, a challenging example with stress concentration is given to compare the described methods. The example is a L-shape plate, as shown in Fig. 8(a). The right side of the plate is fixed and the upper face is applied with a pressure of 1 MPa. The Young's modulus of the plate is 1000 MPa and the Poisson's ratio is 0.3. A uniform mesh of grids is employed as Fig. 8(b) shows.

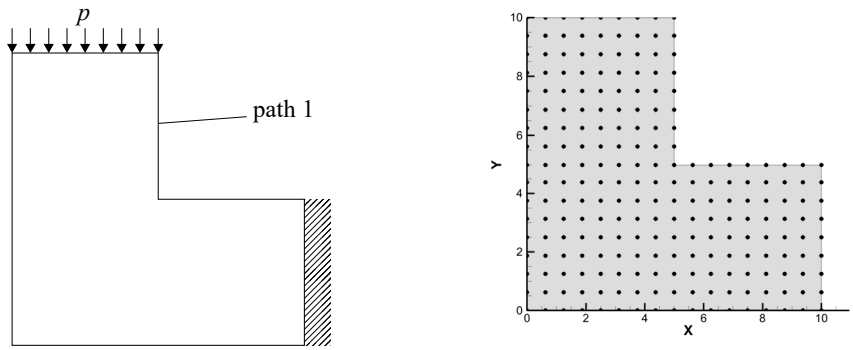

(a) (b)

Figure 8: L-shape plate. (a) Geometry; and (b) Grids.

Figs 9 and 10 show the contours of displacement and von Mises stresses computed by FLM. There are three singular points: the two corners on the right side and the concave corner of the plate. Therefore, the stresses are very large at these corners, as shown in Fig. 10. Figs 11 and 12 compare the displacements and von Mises stresses on the bottom edge computed

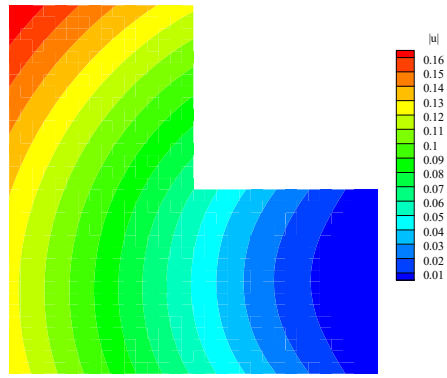

Figure 9: The contours of displacement of the plate.

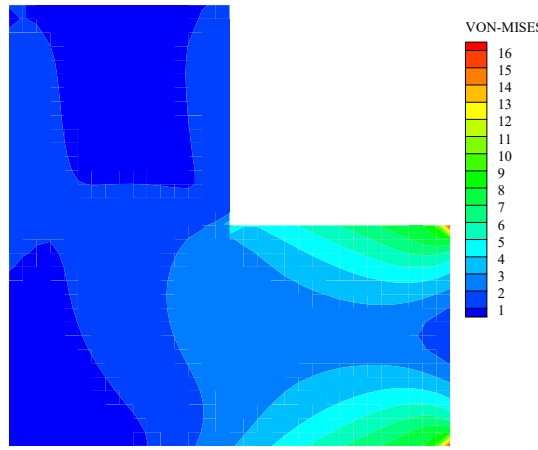

Figure 10: The contours of von Mises stress of the plate.

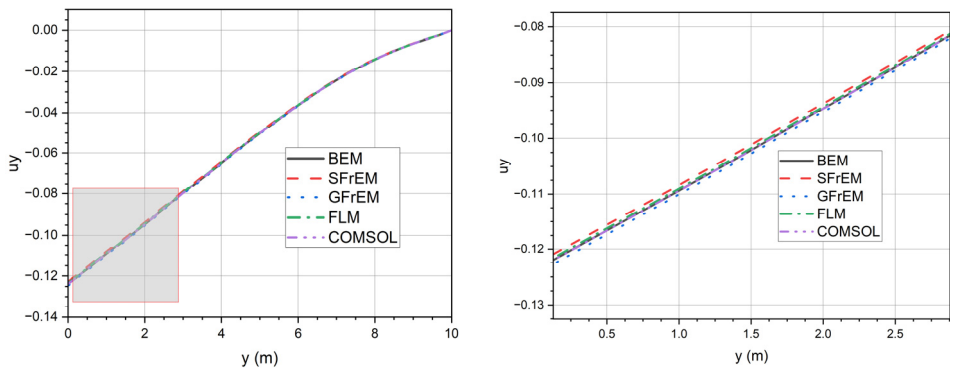

Figure 11: Displacement in y-direction on the bottom edge. (a) Full size; and (b) Local.

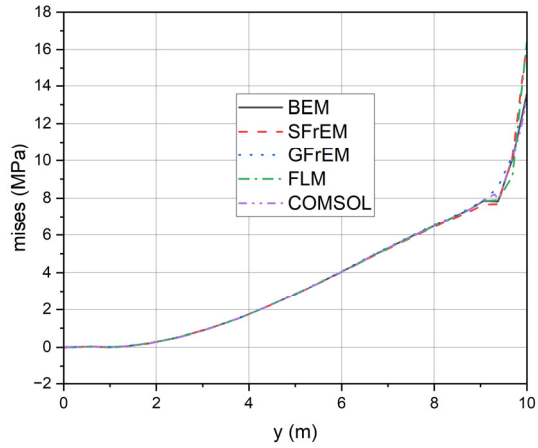

Figure 12: Von Mises stress on the bottom edge.

by different methods. Meanwhile, Figs 13 and 14 compare the displacements and von Mises stresses on path 1. The results of BEM, COMSOL and FLM are almost the same. At the endpoints of the bottom edge and path 1, the displacements of SFrEM are smaller while the displacements of GFrEM are larger than that of BEM and COMSOL. At the singular points, the SFrEM and FLM give larger stresses, which are strong-form schemes.

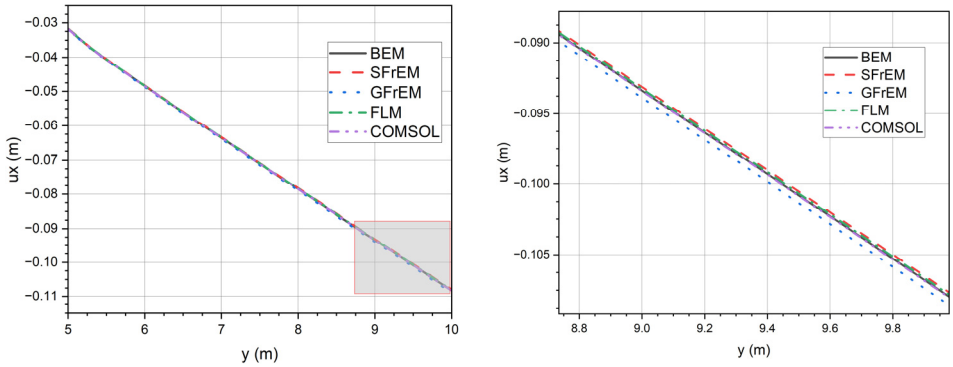

Figure 13: Displacement in y-direction on path 1. (a) Full size; and (b) Local.

7 SUMMARY

In this paper, the progress made in mesh reduction methods of weak-form and strong-form are resumptively described. The focus is on the finite volume method, boundary element method, finite line method and free element method. A numerical example is given for comparison of these methods. The computed results show that all methods can give good results for displacement and the finite line method can simulate the stress concentration more effectively than other method.

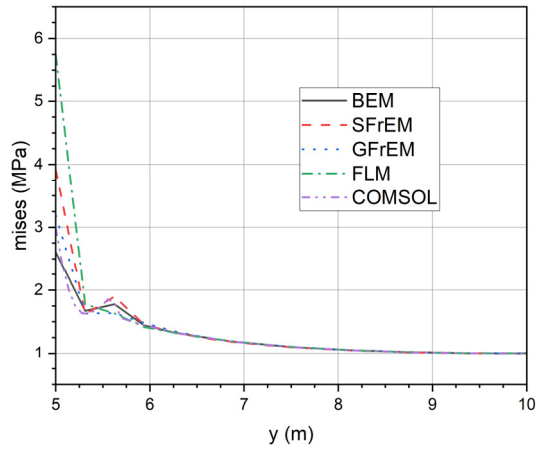

Figure 14: Von Mises stress on path 1.

ACKNOWLEDGEMENT

The support of this investigation by the National Natural Science Foundation of China under Grant No. 12072064 is gratefully acknowledged.

REFERENCES

[1] Coleman, C.J., On the use of radial basis functions in the solution of elliptic boundary value problems. *Comput. Mech*., **17**, pp. 418–422, 1996.

[2] Gao, X.W. et al., Element differential method and its application in thermal-mechanical problems. *International Journal for Numerical Methods in Engineering*, **113**(1), pp. 82–108, 2018.

[3] Hughes, T.J.R., *The Finite Element Method: Linear Static and Dynamic Finite Element Analysis*, Prentice-Hall: Englewood Cliffs, NJ, 1987.

[4] Wen, P.H., Cao, P. & Korakianitis, T., Finite block method in elasticity. *Engineering Analysis with Boundary Elements*, **46**, pp. 116–125, 2014.

[5] Gao, X.W. & Davies, T.G., *Boundary Element Programming in Mechanics*, Cambridge University Press: Cambridge, 2002.

[6] Onate, E., Cervera, M. & Zienkiewicz, O.C., A finite volume format for structural mechanics. *International Journal for Numerical Methods in Engineering*, **37**(2), pp. 181–201, 1994.

[7] Wang, H., Dai, W., Nassar, R. & Melnik, R., A finite difference method for studying thermal deformation in a 3D thin film exposed to ultrashort pulsed lasers. *International Journal of Heat and Mass Transfer*, **51**, pp. 2712–2723, 2006.

[8] Gao, X.-W., Zhu, Y.-M. & Pan, T., Finite line method for solving high-order partial differential equations in science and engineering. *Partial Differential Equations in Applied Mathematics*, **7**, 100477, 2023.

[9] Liu, G.R., An overview on meshfree methods: For computational solid mechanics. *International Journal of Computational Methods*, **13**(5), 1630001, 2016.

[10] Gao, X.W., Gao, L.F., Zhang, Y., Cui, M. & Lv, J., Free element collocation method: A new method combining advantages of finite element and mesh free methods. *Computers and Structures*, **215**, pp. 10–26, 2019.

[11] Fan, C.M., Huang, Y.K., Chen, C.S. & Kuo, S.R., Localized method of fundamental solutions for solving two-dimensional Laplace and biharmonic equations. *Engineering Analysis with Boundary Elements*, **101**, pp. 188–197, 2019.
[12] Ivankovic, A., Demirdzic, I., Williams, J.G. & Leevers, P.S., Application of the finite volume method to the analysis of dynamic fracture problems. *International Journal of Fracture*, **66**(4), pp. 357–371, 1994.
[13] Gong, J., Xuan, L., Ming, P. & Zhang, W., An unstructured finite-volume method for transient heat conduction analysis of multilayer functionally graded materials with mixed grids. *Numerical Heat Transfer, Part B: Fundamentals*, **63**(3), pp. 222–247, 2013.
[14] Moukalled, F., Mangani, L. & Darwish, M., *The Finite Volume Method in Computational Fluid Dynamics: An Advanced Introduction with OpenFOAM® and Matlab*, Springer, 2016.
[15] Cheng, A.H.D., Chen, C.S., Golberg, M.A. & Rashed, Y.F., BEM for theomoelasticity and elasticity with body force: A revisit. *Engineering Analysis with Boundary Elements*, **25**, pp. 377–387, 2001.
[16] Nardini, D. & Brebbia, C.A., A new approach for free vibration analysis using boundary elements. *Boundary Element Methods in Engineering*, ed. C.A. Brebbia, Springer: Berlin, pp. 312–326, 1982.
[17] Gao, X.-W., The radial integration method for evaluation of domain integrals with boundary-only discretization. *Engineering Analysis with Boundary Elements*, **26**, pp. 905–916, 2002.
[18] Linlin, S., Wen, C. & Cheng, A.H.-D., Method of fundamental solutions without fictitious boundary for plane time harmonic linear elastic and viscoelastic wave problems. *Computers and Structures*, **162**, pp. 80–90, 2015.
[19] Zheng, H., Yang, Z., Zhang, C. & Tyrer, M., A local radial basis function collocation method for band structure computation of phononic crystals with scatterers of arbitrary geometry. *Applied Mathematical Modelling*, **60**, pp. 447–459, 2018.
[20] Xu, B.B. et al., Galerkin free element method and its application in fracture mechanics. *Engineering Fracture Mechanics*, **218**(5), 106575, 2019.
[21] Jiang, W.-W. & Gao, X.-W., Analysis of thermo-electro-mechanical dynamic behavior of piezoelectric structures based on zonal Galerkin free element method. *European Journal of Mechanics: A Solids*, **99**, 104939, 2023.